A non-linear viscoelastic model for filled-rubber: analytical formulation, experimental modeling and identification

Jacopo Ciambella[1], Achille Paolone[1], Stefano Vidoli[1]

[1]*Dipartimento di Ingegneria Strutturale e Geotecnica*
Università di Roma "La Sapienza"
Via Eudossiana, 18 - 00184 - Roma, Italy

E-mail: jacopo.ciambella@uniroma1.it, achille.paolone@uniroma1.it, stefano.vidoli@uniroma1.it

Keywords: quasi-linear viscoelasticity, relaxation, creep, hysteresis, identification

1 Introduction

The constitutive behavior of carbon black filled-elastomers is highly nonlinear for what concerns both the quasi-static and the dynamic response. While many contributions have dealt with the modeling of the hyperelastic quasi-static aspects, the attention is focused here on the non-conservative, hysteretic, part of the response, which is a relevant feature for modeling and predicting the energy dissipation in many engineering applications (e.g. rolling resistance of tires, vibration absorbers).

Indeed, carbon black filled-rubber, when loaded with time-dependent external forces, suffer a state of stress which is the superposition of two different aspects: a time independent, *long-term*, behavior (sometimes improperly called "hyperelastic") opposed to a time dependent, *short-term*, response. Step-strain relaxation tests suggest that the short term stresses are larger than the long term or quasi-static ones. Moreover, oscillatory (sinusoidal) tests indicate that dissipative anelastic effects are significant.

Here the effort is focused on reviewing and testing the most used NonLinear Viscoelastic (NLV) models undergoing relaxation, creep and hysteresis tests. To the best knowledge of the authors, no such comparison has yet been made for NLV constitutive relationships, while a similar review has been published for hyperelastic constitutive equations (Hartmann, 2001). Our interest is, hence, focused on experimental/numerical procedure able to efficiently extract the material constitutive parameters. To this end, a brief overview of the macroscale properties of carbon black filled-elastomers is firstly given for the considered dynamic tests. Finally, an experimental procedure is developed for obtaining reproducible, accurate measurements of the viscoelastic parameters, which are then identified by means of an ad-hoc nonlinear optimization algorithm.

2 Constitutive Modeling

In the literature, at least two different approaches are actually followed to model NLV materials. A first formulation is represented by the so-called differential viscoelasticity in which the stress depends on the current values of the strain and strain rate only. This class of constitutive models is generally used to describe finite-amplitude wave propagation. It can reproduce the nonlinear short-term response and the creep behavior, but it fails to catch the long-term material response (e.g., relaxation tests).

A second approach, based on the seminal work of Boltzmann in 1874, relates the stress function to the whole history of deformation via a hereditary integral. Integral type models reproduce all the crucial aspects of rubber behavior (hysteresis, relaxation and creep) and, in addition, their formulation can be developed in a consistent thermodynamic framework. In the simplest situation, the current value of the stress is the sum of two different contributions: a purely elastic term depending

on the current value of the strain and a hereditary integral depending on the strain history. A suitable kernel function in the integral can account for both the short and the long term strain contributions to the current stress value. In this wide sense, this approach can encompass both differential model and fractional-differential models. Because of the inherent nonlinear behavior exhibited by most of carbon black-filled rubber, a linear dependence of the stress response on the strain history is often not applicable. Fung was among the firsts to address this deficiency, proposing the so-called Quasi-Linear Viscoelasticity (QLV) theory (Fung, 1972).

In one dimension, Fung suggested the following relationship for the second Piola-Kirchhoff stress T_{11} and stretch λ

$$T_{11}(t) = T_{11}^{(e)}(\lambda(t)) + \int_0^t \frac{\partial k(t-\tau)}{\partial(t-\tau)} T_{11}^{(e)}(\lambda(s))\mathrm{ds}\,, \tag{1}$$

where $k(t)$ is a suitable relaxation (or kernel) function, $T_{11}^{e}(\lambda)$ is the nonlinearly elastic response function and λ is an axial stretch ratio. Fung's model states that the tensile stress at time t is equal to the instantaneous elastic response T_{11}^{e} decreased by an amount depending on the past history, because $\dot{k}(t)$ is generally assumed as negative.

More recently many investigators have proposed their own version of QLV constitutive relationship. Among them, the equations introduced by Fosdick and Yu (1998), Hallquist (1998), Yang et al. (2000), Shim et al. (2004) and Hibbit et al. (2007) are gathered from Fung's QLV model and, therefore, can properly be compared. In the following, the advantages and drawbacks of each of these models will be discussed.

2.1 Generalized Formulation

First of all let us introduce some notations. We denote by $\mathbf{F} := \partial\mathbf{x}/\partial\mathbf{X}$ the deformation gradient; $\mathbf{x}$ is the position vector in the current configuration of a material particle located at position $\mathbf{X}$ in the reference configuration. The right Cauchy-Green deformation tensor is indicated by $\mathbf{C} := \mathbf{F}^T\mathbf{F}$; the dependence on the time t will be specified only when necessary.

A suitable constitutive equation is a relationship between the second Piola-Kirchhoff stress $\mathbf{T}$ and the strain tensor $\mathbf{C}$. However, from an experimental point of view, it is convenient to express the force recorded during the experiment (divided by the reference cross-section area) in terms of the (nominal) strain. To this end, the constitutive equation can be usefully expressed in terms of the first Piola-Kirchhoff stress $\mathbf{\Pi} := \mathbf{FT}$.

A convenient formulation, to represent the whole set of integral models considered here, is:

$$\mathbf{T}(t) = \mathbf{T}^{(e)}(t) + \mathbf{\Lambda}(t) \int_0^t \frac{\partial k(t-s)}{\partial(t-s)} \mathbf{\Psi}(s,t)\mathrm{ds}\,. \tag{2}$$

Here $\mathbf{T}^{(e)}$ is the instantaneous, purely elastic, stress, $\mathbf{\Lambda}$ and $\mathbf{\Psi}$ are suitable nonlinear function of the current strain and the whole strain history respectively and $k(t)$ is the relaxation function. The same constitutive relation in terms of the first Piola-Kirchhoff stress reads as

$$\mathbf{\Pi}(t) = \mathbf{\Pi}^{(e)}(t) + \mathbf{F}(t)\,\mathbf{\Lambda}(t) \int_0^t \frac{\partial k(t-s)}{\partial(t-s)} \mathbf{\Psi}(s,t)\mathrm{ds}\ , \tag{3}$$

with $\mathbf{\Pi}^{(e)} = \mathbf{FT}^{(e)}$.

The relaxation function k could be represented by a series of simple exponentials, the so-called Prony series, each one with its own relaxation time, e.g.

$$k(t) = 1 + \sum_{i=1}^{N} k_i (e^{-t/\tau_i} - 1)\,, \qquad \sum_{i}^{N} k_i < 1\,; \tag{4}$$

here $\{\tau_i\}$ are the characteristic times (or time constants) and $\{k_i\}$ are normalized scalar coefficients. The number of exponential terms, N, is generally selected to increase the accuracy of the fitting model; in the literature, up to 20 different relaxation times are sometimes used.

The constitutive relation (3) is valid for every NLV material bearing no special characteristic. However carbon black filled-elastomers are usually treated as isotropic and incompressible materials. The first property reflects on the constitutive relationships (2) - (3) requiring all the functions, $\mathbf{T}^{(e)}$, $\mathbf{\Lambda}$ and $\mathbf{\Psi}$, to be isotropic tensor functions of $\mathbf{C}$. In particular, the instantaneous stress, for an incompressible isotropic material, can expressed as

$$\mathbf{\Pi}^{(e)}(t) = \phi_1(I_1(t), I_2(t))\mathbf{F}(t) + \phi_2(I_1(t), I_2(t))\mathbf{F}(t)\mathbf{C}(t)\,, \tag{5}$$

being ϕ_1 and ϕ_2 function of the first two invariants of $\mathbf{C}$ at time t ($I_1 = \mathrm{tr}\{\mathbf{C}\}$, $I_2 = \mathrm{tr}\{\mathbf{C}^{-1}\}$).

The incompressibility constraint ($\det \mathbf{F} = 1$) can be easily taken into account by adding a Lagrange multiplier. Hence, if we introduce the so-called extra stress $\mathbf{\Pi}_{ES}(t)$, Eq. (3) becomes

$$\mathbf{\Pi}(t) = -p(t)\mathbf{F}^{-T}(t) + \mathbf{\Pi}_{ES}(t)\,, \tag{6}$$

where $p(t)\mathbf{F}^{-T}(t)$ is an arbitrary non-constitutive constraint reaction stress. Finally, the constitutive equations for the extra stress are

$$\begin{aligned} \mathbf{\Pi}_{ES}(t) &= \mathbf{\Pi}_{ES}^{(e)} + \mathbf{F}(t)\,\mathbf{\Lambda}(t) \int_0^t \frac{\partial k(t-s)}{\partial (t-s)} \mathbf{\Psi}(s,t)\mathrm{ds}\,, \\ \mathbf{\Pi}_{ES}^{(e)}(t) &= \phi_1(t)\mathbf{F}(t) + \phi_2(t)\mathbf{F}(t)\mathbf{C}(t)\,. \end{aligned} \tag{7}$$

Within this general setup, a suitable choice of the instantaneous stress $\mathbf{\Pi}_{ES}^{(e)}$ and of the functions $\mathbf{\Lambda}$, and $\mathbf{\Psi}$ in Eqs. (7) permit to obtain all the models under investigation. In particular, with

$$\mathbf{\Lambda}(t) = \mathbf{I}, \qquad \mathbf{\Psi}(s,t) = \mathbf{F}^{-1}(s)\mathbf{\Pi}_{ES}^{(e)}(s)\,, \tag{8}$$

Eq. (6) reduces to Fung's constitutive equation (Fung, 1972). Here and henceforth $\mathbf{I}$ represents the 3x3 identity matrix.

Table 1 summarizes the choice of the parameters $\mathbf{\Pi}_{ES}^{(e)}$, $\mathbf{\Lambda}$ and $\mathbf{\Psi}$ for each of the selected constitutive equations. With the intent of having the same number of parameters for the instantaneous stress $\mathbf{\Pi}_{ES}^{(e)}$ of each model, a Mooney-Rivlin representation has been chosen for the models 1, 2, 3 and 6, in which the constitutive assumption regarding $\mathbf{\Pi}^{(e)}$ were not specified by the authors. Moreover, models 2, 4, 5, in their original versions, had a single relaxation time ($N = 1$), which has revealed unable to fit the experimental data under investigation. A Prony's series with 2, or more, exponential terms was alternatively used.

The constitutive equations 3 and 6 are those implemented in the Abaqus FEA and LS-Dyna codes respectively. These numerical tools are often called upon to simulate the behavior of complex NLV systems, hence is essential to compare those models with the others from literature. Indeed, the Abaqus model in Tab. 1 is written in the special case of simple tension, which is the experimental situation considered here.

Table 1: Material models based on the proposed generalized formulation.

	Model Name	$\mathbf{\Pi}_{ES}^{(e)}$ ϕ_1	ϕ_2	$\mathbf{\Lambda}$	$\mathbf{\Psi}$
1	Fung	$2\left[\alpha_1+\alpha_2 I_1(t)\right]$	$-2\,\alpha_2$	$\mathbf{I}$	$\mathbf{F}^{-1}(s)\mathbf{\Pi}_{ES}^{(e)}(s)$
2	Fosdick and Yu	$2\left[\alpha_1+\alpha_2 I_1(t)\right]$	$-2\,\alpha_2$	$\mathbf{C}^{-1}(t)$	$\beta_1\left[\mathbf{C}(s)\mathbf{C}^{-1}(t)-\mathbf{I}\right]$
3	Hallquist	$2\left[\alpha_1+\alpha_2 I_1(t)\right]$	$-2\,\alpha_2$	$\mathbf{I}$	$-\beta_1\dot{\mathbf{C}}(s)$
4	Yang et al.	α_1	α_2	$\mathbf{I}$	$-\left[\beta_1+\beta_2 I_2(s)\right]\dot{\mathbf{C}}(s)$
5	Shim et al.	α_1	α_2	$\left[1+\gamma_1\dot{I}_2(t)\right]\mathbf{I}$	$-\left[\beta_1\frac{\dot{I}_1(s)}{I_1(s)}\mathbf{C}(s)+2\beta_2\dot{\mathbf{C}}(s)\right]$
6	Hibbit et al.	$2\left[\alpha_1+\alpha_2 I_1(t)\right]$	$-2\,\alpha_2$	$\mathbf{I}$	$\mathbf{F}^{-1}(s)\mathbf{\Pi}^{(e)}(s)\mathbf{C}(s)\mathbf{C}^{-1}(t)$

3 Experimental Set-up

The problem of determining the set of experiments to correctly estimate the coefficients of a NLV model is a challenging engineering task. Testing procedures which are both highly-repeatable, standardizable and not-time consuming are required.

Standard dynamic tests for elastomers, which are based on small harmonic deformations superimposed on a large static displacement, have to be repeated for every frequency and every amplitude of interest; therefore, they require a considerable amount of time to be performed. Moreover, very precise, thus expensive, machineries are necessary to reach the higher frequencies of interest. Relaxation, creep and cyclic tests, all in compression, have consequently been preferred in this investigation.

The material objective of this study was a carbon black-filled rubber compound, provided by the Bridgestone Firestone Technical Center Europe s.p.a. in Rome. Further details on the material, especially the content and the type of the carbon black and which rubbers were used can unfortunately not be given as they are not known to the authors.

Experiments were conducted with a Zwick/Roell z010. The specimen was cylindrical shaped with diameter-to-height ratio D/H = 0.76. During all the experiment the plate were kept lubricated with graphite to guarantee uniform lateral displacement over the height and, consequently, avoid bulging of the mantle surface due to no-slip at the interfaces between the top and bottom surfaces with the contact surfaces of the support and load devices. Therefore, the strain field could be reasonably assumed uniform along the specimen. This is particularly important since the material exhibits highly nonlinear behavior: constitutive nonlinearities coupled with nonuniform strain would be difficult, even impossible, to analyze. All the tests were conducted without temperature control, so the specimen could be plausibly assumed at room temperature which was 25 °C. All the samples were subjected to a cyclic strain up to $25\,\%$ to account for Mullins' effect.

The stress relaxation test were performed at constant strain of $17\,\%$ ($\lambda = 0.83$). The specimen was conducted to this state from the initial configuration ($\lambda = 1$) with a ramp history wherein the strain increases along a (nearly) constant strain rate path up to a time $t_0 = 0.7$ s until the

constant strain level is reached. The resulting stress relaxation curve is represented by the thick line in Fig. 1a. In this scenario the ideal step-strain relaxation function, which has an infinite initial slope, is approached only asymptotically; indeed, the effects of a finite strain rate are more significant for initial times.

The laboratory environments normally imposes a range for the observable time scales. The highest sampling rate the acquisition channel can reach determines the shortest achievable time; besides the duration of the experiment is an upper bound for time scales. The Zwick/Roell z010 equipment is able to acquire data up to the frequency $10\,\mathrm{kHz}$; $1\,\mathrm{kHz}$ was used, whereas the experiments lasts $30\,\mathrm{s}$. This choice was a compromise between the minimum observable time scale and number of data samples recorded.

Relaxation tests permit to capture the material behavior involving larger time scales. Since in many engineering applications (e.g., tires, engine mounts, etc.), the shortest intrinsic times are more significant, hysteresis loop at high strain rate was also performed. The loading/unloading path was repeated for four different velocity and is given in Fig. 3 (thick line).

During the loading path the experiment was monitored exerting a displacement from the undeformed configuration ($\lambda = 1$) up to the strain 0.83 with constant strain rate. The unloading path was force driven with a constant stress rate up to the null force ($0\,\mathrm{N}$). Since elastomers have an intrinsic viscous behavior, after the unloading, the strain corresponding to the stress free configuration (null exerted force) was not zero, at least initially. To permit the material to recover the initial state, which was both zero force and zero strain, the zero force final position after the unloading was maintained for $3\,\mathrm{s}$, while the displacement was monitored. This, indeed, corresponds to a creep test. At the end of this waiting time the undeformed, stress-free, configuration was reached again.

The experimental results described above can properly be modeled by means of the solution of extension/compression of a cylindrical body subjected to incompressibility. Since for all the experiments the deformation can reasonably be assumed uniform along the specimen, the homogeneous motion is described by

$$x_1 = \lambda(t) X_1, \qquad x_2 = \lambda(t)^{-1/2} X_2, \qquad x_3 = \lambda(t)^{-1/2} X_3 \tag{9}$$

where $\lambda(t)$ (≤ 1) is the stretch ratio in the direction of the uniaxial compression $\Pi_{11}(t)$. The resulting deformation gradient has the diagonal form

$$\mathbf{F}(t) = \mathrm{Diag}\left[\lambda(t), \lambda(t)^{-1/2}, \lambda(t)^{-1/2}\right] . \tag{10}$$

Vanishing of the lateral stresses $\Pi_{22}(t) = \Pi_{33}(t) = 0$ determines the Lagrange multiplier $p(t)$, and elimination of $p(t)$ yields

$$\begin{aligned}\Pi_{11}(t) =& \Pi^{(e)}_{ES\,11}(t) - \lambda^{-3/2}(t)\,\Pi^{(e)}_{ES\,33}(t) + \lambda(t)\,\Lambda_{11}(t) \int_0^t \frac{\partial k(t-s)}{\partial(t-s)} \Psi_{11}(s,t)\mathrm{ds} \\ & - \lambda^{-2}(t)\,\Lambda_{33}(t) \int_0^t \frac{\partial k(t-s)}{\partial(t-s)} \Psi_{33}(s,t)\mathrm{ds}\,,\end{aligned} \tag{11}$$

for the generalized model (6). Note that inertial forces have been neglected in comparison with the internal stresses. Equation (11) will be used in the next section to identify the constitutive parameters for each model under investigation.

4 Identification of Material Parameters

The standard procedure used to identity constitutive parameters in an integral type viscoelastic relationship strongly relies on the fact that the stress response could be usefully decompose in two contributions: a short term response which asymptotically tends towards the instantaneous response, for increasing strain rate, and a long-term contribution. If the material behaves as linear viscoelastic, these two effects could easily be decoupled and the identification problem could be solved for the two problems independently; however, in the present nonlinear case, a joined identification problem must be addressed in which both short and long-term contributions determine the whole set of material parameters.

The identification of the constitutive parameters relies on the minimization of an appropriate weighted norm function which takes into account for the different properties of the material response discussed above. To this end, the stress time history is splitted in the short-term contribution ($\widehat{\Pi}_{11}^S$, $\widetilde{\Pi}^S$), corresponding to the time instants with highest values of acceleration, and in the long-term one ($\widehat{\Pi}_{11}^L$, $\widetilde{\Pi}^L$), corresponding to the remaining time. The resulting minimization problem can be expressed as

$$\min_{\alpha_i,\beta_i,k_i,\tau_i} f(\alpha_i,\beta_i,k_i,\tau_i)\,, \tag{12}$$

where

$$f(\alpha_i,\beta_i,k_i,\tau_i) = m_1 \left\|\widehat{\Pi}_{11}^S - \widetilde{\Pi}^S\right\|_2^2 + m_2 \left\|\widehat{\Pi}_{11}^L - \widetilde{\Pi}^L\right\|_2^2 + n_1 \left\|\widehat{\Pi}_{11}'^S - \widetilde{\Pi}'^S\right\|_2^2 + n_2 \left\|\widehat{\Pi}_{11}'^L - \widetilde{\Pi}'^L\right\|_2^2,$$

and m_1, m_2, n_1 and n_2 are scalar weights, $\widehat{\Pi}_{11}^S$, $\widehat{\Pi}_{11}^L$, $\widehat{\Pi}_{11}'^S$ and $\widehat{\Pi}_{11}'^L$ are the discrete stress and its derivative computed from the model, while $\widetilde{\Pi}^S$, $\widetilde{\Pi}^L$, $\widetilde{\Pi}'^S$ and $\widetilde{\Pi}'^L$ the measured counterparts. The norm of derivatives in (12) has been introduced to obtain a better material stiffness evaluation.

The functional dependence of f on $\{\tau_i\}$ is highly nonlinear, hence the resulting minimization problem (12) is nonconvex. To overcome the numerical difficulties related to the presence of multiple minima, the characteristic times are fixed a-priori, say $\overline{\tau}_i$, in a suitable time range. In particular, the initial time interval is selected considering the duration of experiment as an upper bound for $\{\tau_i\}$ and the sampling rate as a lower bound; within this range, five time constants are initially chosen to be equally spaced in logarithmic scale. The resulting reduced minimization problem is

$$\min_{\alpha_i,\beta_i,k_i} f(\alpha_i,\beta_i,k_i,\overline{\tau}_i)\,. \tag{13}$$

Since characteristic times of carbon black filled-elastomers are well-known to be very close to each other, after a first tentative solution of (13), an iterative scheme to refine the relaxation times is applied. It consists of the following step:

1. the characteristic times $\{\tau_i^{(l)}\}$ at iteration l are discarded if the corresponding scalar coefficients $\{k_i^{(l)}\}$ are below a chosen threshold $\overline{k}$. If $k_i^{(l)} \geq \overline{k}$, $\tau_i^{(l)}$ at the successive step is splitted into
$$\tau_i^{(l+1)} = \{\tau_i^{(l)}\, 10^{-(\frac{\Delta}{3})^l}, \tau_i^{(l)}, \tau_i^{(l)}\, 10^{(\frac{\Delta}{3})^l}\}\,, \tag{14}$$
where Δ is the logarithmic distance between the time constants at iteration 0;

2. the reduced minimization problem is solved for the new set of time constants $\{\tau_i^{(l+1)}\}$.

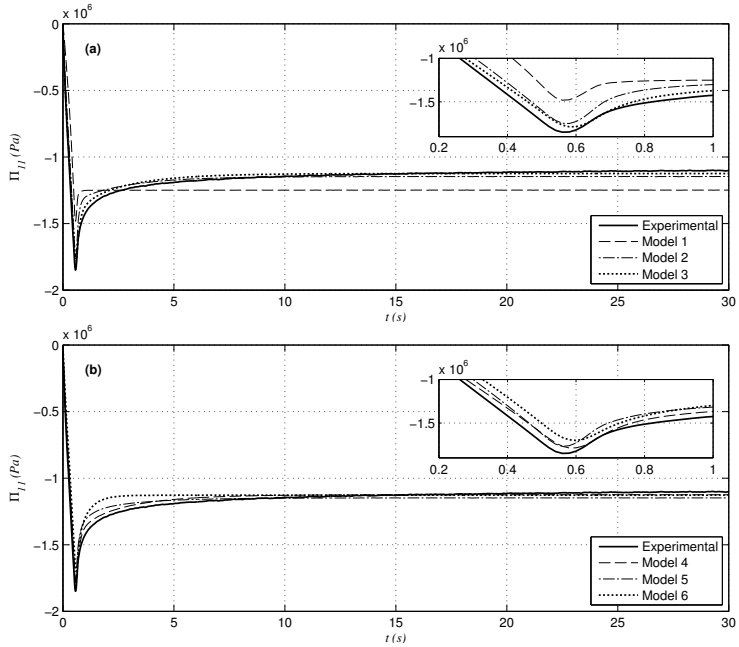

Figure 1: Identified normal stresses Π_{11} versus time t for relaxation experiment after two steps of the proposed identification procedure. In the nested graph, the same plot is sketched in the range $t \in [0.2, 1]$.

The algorithm terminates when all the scalar coefficients $\{k_i\}$ exceed $\overline{k}$. A derivative free algorithm (direct-search method) was used at each step for the solution of (13). Since the functional f is nonlinear, a good starting point for the algorithm is needed. In the present case, the starting point at step $l+1$ is taken to be the solution at the previous step $(\alpha_i^{(l)}, \beta_i^{(l)}, k_i^{(l)})$; the initial value of the scalar coefficients $k_i^{(l+1)}$, corresponding to the newly added time constants, are set to zero.

In the next paragraph, the results of the iterative identification procedure will be presented and discussed for all the models under investigation.

5 Results and Conclusions

We firstly report on the results of the identification procedure applied to the models in Tab. 1 for relaxation and finite loop tests.

All the models are able to describe the behavior undergoing relaxation tests also with the lower number of time constants ($N = 2$ in the present case). Fung's model (model 1 in Tab. 1) cannot properly describe the relaxation curve. In particular, the slope of the curve around the kink in the stress function is completely missed; as it will be clear later, this fact influences the prediction of the energy dissipation.

Figure 2 shows the effects of the iterative procedure on the fitting results. While there is not any appreciable improvement for model 1, the final value of the objective function (13) for model 4 passes from 8.0×10^{-2} of the first iteration to 2.4×10^{-2} of the third iteration with a reduction of $68\,\%$ for the first two steps. A similar result has been obtained for all the other models, but is not showed here.

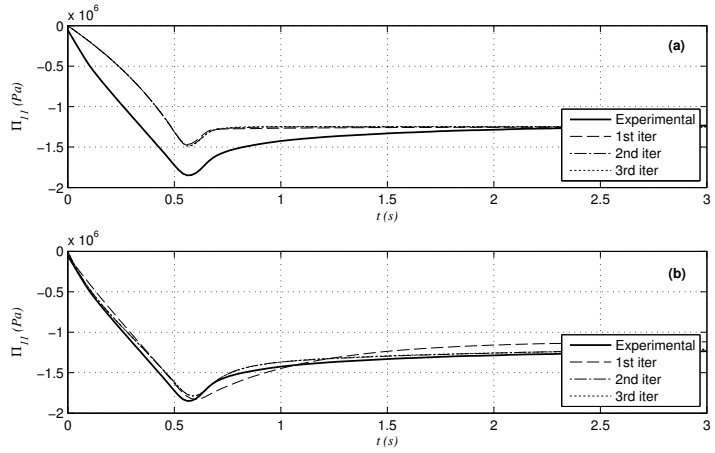

Figure 2: Normal stresses Π_{11} versus time t in the range $t \in [0, 3]$ for Model 1 - panel **(a)** - and Model 4 - panel **(b)**. There is an improvement in the fitting from the first to the third iteration for Model 4 but not for Model 1.

The results of the iterative fitting for the cyclic loops at different strain rate are reported in Fig. 3 in the case of 6 relaxation times. A good agreement between the experimental data and the fitting models seems to be reached. However, the stress-strain plots reported in Figs. 5a and 5b show up the capability of each model in describing the energy dissipation. While model 1 completely misses the dissipated energy at the highest strain rate and model 6 cannot properly describe the initial stiffness, the other models catch the qualitative behavior of the material.

The poor performance of Fung's model (model 1) could be imputable to the coupling between the elastic instantaneous stress and the integrand of the dissipative part, which have the same coefficients. By modifying Fung's constitutive equation to have different coefficients in the two terms, a slightly improvement of the fitting model has been obtained but the results are still not comparable with the other models under investigation.

As soon as the strain rate of the loading path increases, hence the highest time constants become

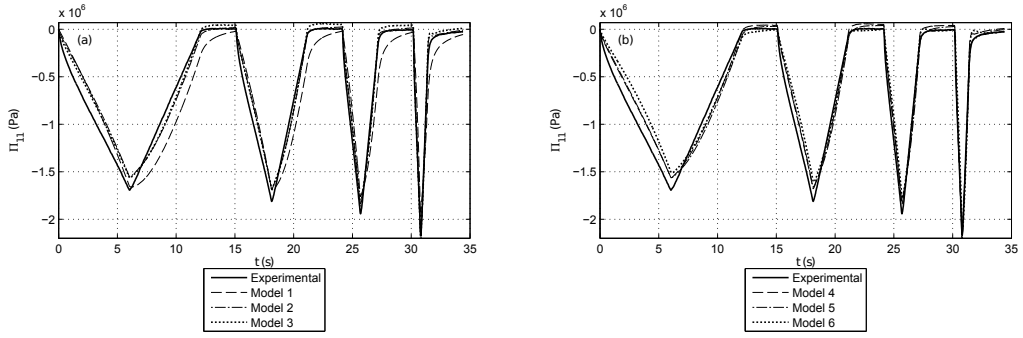

Figure 3: Identified normal stresses Π_{11} versus time t for hysteresis experiment after two steps of the proposed identification procedure.

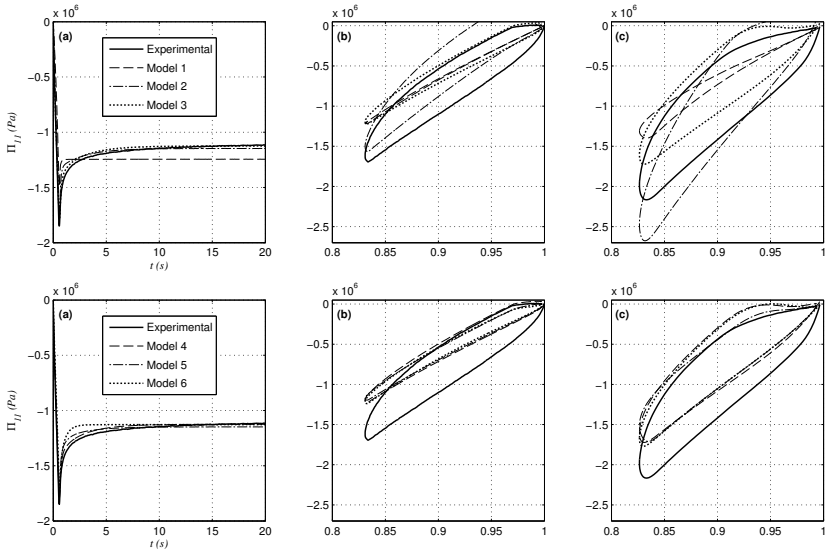

Figure 4: Panel **(a)** shows the identified normal stresses Π_{11} versus time t for relaxation experiment. Panels **(b)** and **(c)** are the hysteresis loop at $\dot{\lambda} = 0.03$ and $\dot{\lambda} = 0.3$, respectively, predicted from the coefficients identified through the relaxation test.

more significant, a considerable improvement in the fitting is obtained. The material stiffness during the loading path is well-described by all the models except model 1, while the most accurate description of the unloading stiffness is given by model 5.

For a more accurate comparison and to properly highlight advantages and drawbacks, the predictability of each model has to be evaluated. To this end, the behavior of the material under finite loop tests is predicted from the coefficients identified through relaxation test and viceversa (Figs. 4b and 4c; Fig. 5c). In the first case, even if the relaxation curve is well-described by most of the models, the dissipated energy in cyclic loop tests is underestimated for all the models except model 2, which misses the material stiffness at the higher strain rates (Fig. 4c). Figure 5c shows that all the models overestimate the value of the stress at higher time instants of at least $30\,\%$.

In conclusions, the present comparison has revealed that models 2, 3, 4 and 5 are able to qualitatively describe the behavior of the rubber-like material under investigation, even if they cannot properly catch the dissipated energy undergoing the deformation process, especially at lower strain rate. Fung's model (model 1), firstly introduced to describe the behavior of soft biological tissues, has revealed completely unable to describe the dissipation properties both at higher and lower strain rates; model 6, instead, has produced a fitting model which underestimates the material stiffness at very low strain in all the considered experimental cases. Since, in many engineering applications, the material is subjected to a strain lower than $10\,\%$, a relevant stiffness error within this range should be consider a serious drawback for the model.

References

R. Fosdick and J. H. Yu. Thermodynamics, stability and non-linear oscillations of viscoelastic solids .2. History type solids. *Internat. J. Non-Linear Mech.*, 33(1):165–188, January 1998.

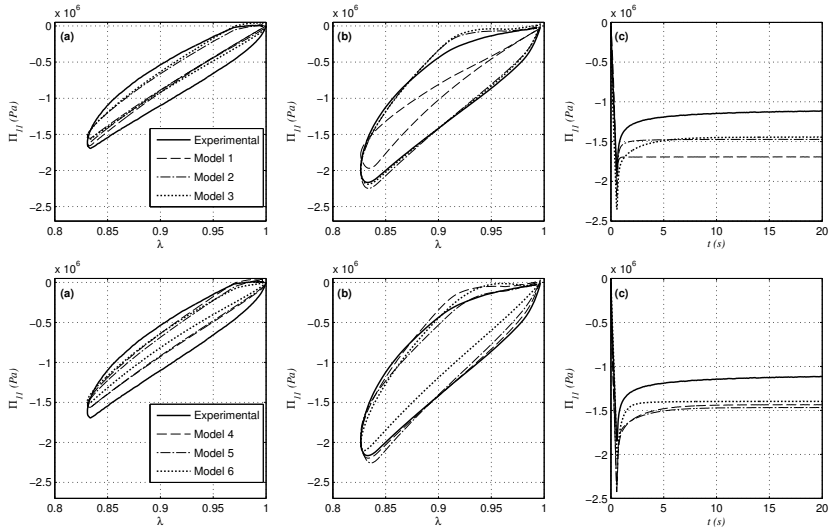

Figure 5: Panels **(a)** and **(b)** show the identified normal stresses Π_{11} versus time t for cyclic experiment at $\dot{\lambda} = 0.03$ and $\dot{\lambda} = 0.3$ respectively. Panel **(c)** is the relaxation curve predicted from the coefficients identified through the hysteresis loops.

Y. C. Fung. Stress-strain-history relations of soft tissues in simple elongation. In N. Perrone Y.C. Fung and M. Anliker, editors, *Biomechanics: Its Foundations and Objectives*, pages 181–208. Prentice Hall, Englewood Cliffs, NJ, 1972.

J. Hallquist. *LS-DYNA theoretical manual*. Livermore Software Technology Corporation, 1998.

S. Hartmann. Numerical studies on the identification of the material parameters of Rivlin's hyperelasticity using tension-torsion tests. *Acta Mechanica*, 148(1-4):129–155, 2001.

D. Hibbit, B. Karlsson, and P. Sorensen. *ABAQUS/Theory Manual*. Hibbitt, Karlsson & Sorensen, Inc., Rhode Island, 6.7 edition, 2007.

V. P. W. Shim, L. M. Yang, C. T. Lim, and P. H. Law. A visco-hyperelastic constitutive model to characterize both tensile and compressive behavior of rubber. *J. Appl. Polym. Sci.*, 92(1):523–531, April 2004.

L. M. Yang, V. P. W. Shim, and C. T. Lim. A visco-hyperelastic approach to modelling the constitutive behaviour of rubber. *International Journal of Impact Engineering*, 24(6-7):545–560, July 2000. ISSN 0734-743X.